
GENERALIZED TCP-RED DYNAMICAL MODEL FOR INTERNET CONGESTION CONTROL

A PREPRINT

José M. Amigó, Guillem Duran, Angel Giménez, Oscar Martínez-Bonastre and José Valero

Centro de Investigación Operativa,
Universidad Miguel Hernández de Elche,
Avda. de la Universidad s/n, 03202 Elche, Spain

jm.amigo@umh.es, guillem@fragile.tech, a.gimenez@umh.es, oscar.martinez@umh.es, jvalero@umh.es

January 23, 2025

ABSTRACT

Adaptive management of traffic congestion in the Internet is a complex problem that can gain useful insights from a dynamical approach. In this paper we propose and analyze a one-dimensional, discrete-time nonlinear model for Internet congestion control at the routers. Specifically, the states correspond to the average queue sizes of the incoming data packets and the dynamical core consists of a monotone or unimodal mapping with a unique fixed point. This model generalizes a previous one in that additional control parameters are introduced via the data packet drop probability with the objective of enhancing stability. To make the analysis more challenging, the original model was shown to exhibit the usual features of low-dimensional chaos with respect to several system and control parameters, e.g., positive Lyapunov exponents and Feigenbaum-like bifurcation diagrams. We concentrate first on the theoretical aspects that may promote the unique stationary state of the system to a global attractor, which in our case amounts to global stability. In a second step, those theoretical results are translated into stability domains for robust setting of the new control parameters in practical applications. Numerical simulations confirm that the new parameters make it possible to extend the stability domains, in comparison with previous results. Therefore, the present work may lead to an adaptive congestion control algorithm with a more stable performance than other algorithms currently in use.

Keywords Congestion control in the Internet · Adaptive queue management · Random early detection · Discrete-time dynamical systems · Global stability · Robust setting of control parameters

1 Introduction

With the increasing number of users and application services, the traffic congestion control on the Internet has become a timely topic both for communication engineers and applied mathematicians. Indeed, poor management of traffic congestion may result in loss of information and be detrimental to the performance of applications [1]. To prevent this from occurring, several congestion control algorithms are executed at the sources (called transmission control protocols, TCPs) and at the routers. How to stabilize the router queue length around a desired target regardless of the traffic loads is an open problem of congestion control and the main concern of this paper. Most of the current algorithms implement early detection of the congestion, along with feedback signaling and reconfiguration of the control parameters, to avoid the build up of instabilities such as abrupt fluctuations of the buffer occupancy, not to mention a service disruption. These aptly called Adaptive Queue Management (AQM) mechanisms are predominantly based on stochastic models, and include Random Early Detection [2], Random Early Marking [3], and Adaptive Virtual Queue [4]. Time averaging also allows formulating congestion control mechanisms in the language of deterministic dynamical systems, whether discrete-time or continuous-time, thus offering an interesting and promising alternative to conventional approaches. This paper deals precisely with such dynamical models in discrete time.

Random early detection (RED) was one of the first proposed AQM mechanisms. In a nutshell, RED drops incoming data packets with a probability that depends on an average between the past average queue size and the current queue size (see Section 2 for more details). In [5] Ranjan et al. reformulated RED as a one-dimensional discrete-time dynamical system, with the average queue sizes being the states. This model splits the state interval into three segments; the dynamics is affine in the left segment, \cup -convex with a unique fixed point in the middle one, and linear in the right one, where the middle segment is a sink (trapping region) of the global dynamics when it is invariant. Moreover, Ranjan et al. found that their model undergoes direct and reverse bifurcations with respect to several control parameters of the model. Not surprisingly, these bifurcation scenarios exhibit period-doubling transitions to chaos and positive Lyapunov exponents, as it is well known from unimodal (one-humped) mappings, e.g., the quadratic family $x \mapsto \lambda x(1-x)$, $0 < \lambda \leq 4$, mapping the interval $[0, 1]$ into itself [6, 7]. This being the case, a stable congestion control calls for sidestepping those ranges of the control parameters where the dynamics is chaotic or just periodic.

In [8] and [9] the authors proposed a generalization of the above RED nonlinear model with improved stability. Our dynamical model features a probability distribution for the data packet dropping with two additional parameters α and β (the beta distribution), which boosts the controllability of the RED dynamics. Indeed, we showed in [8] that, for adequately chosen α and β , the stability ranges of some key parameters extend beyond their bifurcation values in the original formulation [5], which corresponds to $\alpha = \beta = 1$. In [9] we surveyed numerically the stability regions in parametric space to locate robust settings of α and β . Yet, the major issue of the paper at hand are the theoretical underpinnings of the proposed generalized RED model in order to understand the numerical results and anticipate the response of the system under different parameter configurations. This is also a necessary step on the way to a full-fledged implementation of the ensuing AQM mechanism that takes into account the real-time variation of some system parameters (notably, the number of users). For other approaches to RED stabilization, see [10, 11, 12, 13].

Bearing the above objectives in mind, this paper focuses on the basic properties of the generalized RED dynamics and their application to find robust ranges of the control parameters α and β that guarantee a stable dynamics (meaning that the unique fixed point is a global attractor). The relation between theory and application is bidirectional: the choice and generality of the theoretical results correlates with the application sought. Thus, we do not delve into the chaotic properties of the RED dynamics. Technical details are also beyond the scope of this paper.

The remaining sections are organized as follows. After a brief description in Section 2 of the dynamical model for RED proposed by Rajan et al. [5], a generalization along the lines explained above is presented in Section 3, analyzed in Sections 4 (basic dynamical properties) and 5 (local stability), and illustrated in Section 6 with a few examples. Section 7 is central to this paper. There we study the global stability of the generalized RED dynamical model presented in Section 3, tailored to monotonic (Section 7.1) and unimodal (Section 7.2) dynamics in the trapping region. In so doing we look for theoretical results that can be implemented in an actual control algorithm. Application of the results of Section 7 to the tuning of the new control parameters α and β , as well as other practical issues, is the subject of Section 8. Results requiring numerical simulations have been grouped in Section 9. They comprise a benchmarking of our generalized model against the conventional one that favors our model (Section 9.1), and a survey of stability robustness in the (α, β) -parametric space (Section 9.2), followed by a short discussion (Section 9.3). The final section contains the conclusion and outlook.

2 A RED dynamical model

Figure 1 depicts the communication network we consider throughout: N users are connected to a Router 1 which shares an internet link with Router 2. The capacity of this channel is C . Further parameters of the system are the packet size M , the round-trip time (propagation delay) d of the packets, and the buffer size B of R1.

In the RED model, the probability p of dropping an incoming packet at the router depends on the average queue size q^{ave} as follows:

$$p(q^{\text{ave}}) = \begin{cases} 0 & \text{if } q^{\text{ave}} < q_{\min}, \\ 1 & \text{if } q^{\text{ave}} > q_{\max}, \\ \frac{q^{\text{ave}} - q_{\min}}{q_{\max} - q_{\min}} p_{\max} & \text{otherwise.} \end{cases} \quad (1)$$

Thus, q_{\min} and q_{\max} are the lower and upper threshold values of q^{ave} for accepting and dropping an incoming packet, respectively, and p_{\max} is the selected drop probability when $q^{\text{ave}} = q_{\max}$, i.e., the maximum packet drop probability. The average queue size is updated at the time of the packet arrival according to the averaging

$$q_{\text{new}}^{\text{ave}} = (1 - w)q_{\text{old}}^{\text{ave}} + wq^{\text{cur}} \quad (2)$$

between the previous average queue size $q_{\text{old}}^{\text{ave}}$ and the current queue size q^{cur} , where $0 < w < 1$ is the *averaging weight*. The higher w , the faster the RED mechanism reacts to the actual buffer occupancy. In practice w is taken rather small, typically $\lesssim 0.2$ [14].

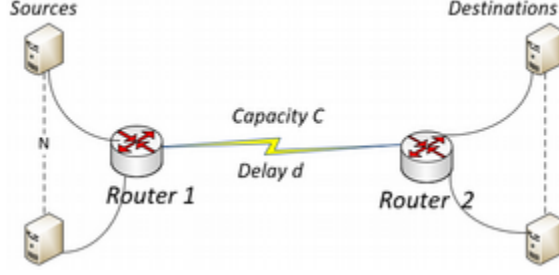


Figure 1: Network topology (source [8]).

Based on RED, Ranjan et al. [5] derived the following “discrete-time feedback model for TCP-RED” (with a slight change in notation):

$$q_{n+1}^{\text{ave}} = \begin{cases} (1-w)q_n^{\text{ave}} & \text{if } q_n^{\text{ave}} \geq \theta_r, \\ (1-w)q_n^{\text{ave}} + wB & \text{if } q_n^{\text{ave}} \leq \theta_l, \\ (1-w)q_n^{\text{ave}} + w\left(\frac{NK}{\sqrt{p_n}} - \frac{Cd}{M}\right) & \text{otherwise,} \end{cases} \quad (3)$$

where $0 \leq q_n^{\text{ave}} \leq B$ is the average queue size at time $n = 0, 1, \dots$, K is a constant between 1 and $\sqrt{8/3}$ (usually $\sqrt{3/2}$) [15],

$$p_n = \frac{q_n^{\text{ave}} - q_{\min}}{q_{\max} - q_{\min}} p_{\max}, \quad (4)$$

and the left and right thresholds $q_{\min} < \theta_l < \theta_r \leq q_{\max}$ are given, respectively, by

$$\theta_l = \frac{q_{\max} - q_{\min}}{p_{\max}} \left(\frac{NMK}{BM + Cd} \right)^2 + q_{\min} \quad (5)$$

and

$$\theta_r = \begin{cases} \frac{q_{\max} - q_{\min}}{p_{\max}} \left(\frac{NMK}{BM} \right)^2 + q_{\min} & \text{if } p_{\max} \geq \left(\frac{NMK}{Cd} \right)^2, \\ q_{\max} & \text{otherwise.} \end{cases} \quad (6)$$

In order that $\theta_l < \theta_r$ also when $\theta_r = q_{\max}$, it is necessary that

$$\left(\frac{NMK}{BM + Cd} \right)^2 < p_{\max}, \quad (7)$$

hence

$$\left(\frac{NMK}{Cd} \right)^2 < \left(1 + \frac{BM}{Cd} \right)^2 p_{\max}. \quad (8)$$

According to (2), θ_l is the largest average queue size such that $q_n^{\text{ave}} \leq \theta_l$ implies $q_{n+1}^{\text{cur}} = B$. Likewise, θ_r is the smallest average queue size such that $q_n^{\text{ave}} \geq \theta_r$ implies $q_{n+1}^{\text{cur}} = 0$.

Ranjan et al. showed also in [5] that the dynamical system defined in (3) can be chaotic depending on the parameter settings. Therefore, a stability analysis of this system is needed in order to identify regions in parameter space where the dynamic is stable. This will be done in the next sections with a more general model. For a continuous-time nonlinear model for RED, see [16].

3 A generalized RED dynamical model

For notational convenience we shorten henceforth q^{ave} to q , and introduce the dimensionless constants

$$A_1 = \frac{NK}{\sqrt{p_{\max}}}, \quad A_2 = \frac{Cd}{M}. \quad (9)$$

Condition (7) translates then into

$$\left(\frac{A_1}{A_2 + B} \right)^2 = \frac{1}{p_{\max}} \left(\frac{NMK}{BM + Cd} \right)^2 < 1, \quad (10)$$

and condition (8) into

$$\left(\frac{A_1}{A_2}\right)^2 = \frac{1}{p_{\max}} \left(\frac{NMK}{Cd}\right)^2 < \left(1 + \frac{BM}{Cd}\right)^2 = \left(1 + \frac{B}{A_2}\right)^2. \quad (11)$$

Proposition 1 *The constants A_1 and A_2 of the RED model are subject to the constraint*

$$A_1 < A_2 + B. \quad (12)$$

Inequality (12) is assumed to hold throughout this paper.

In [8] we generalized the RED dynamical model (3) by replacing the probability law (4) by

$$p_n = I_{\alpha,\beta}(z(q_n)) \cdot p_{\max}, \quad (13)$$

where $I_{\alpha,\beta}(x)$, $0 \leq x \leq 1$, is the beta distribution function (or normalized incomplete beta function),

$$I_{\alpha,\beta}(x) = \frac{\mathfrak{B}(x; \alpha, \beta)}{\mathfrak{B}(1; \alpha, \beta)}, \quad \mathfrak{B}(x; \alpha, \beta) = \int_0^x t^{\alpha-1}(1-t)^{\beta-1} dt, \quad (14)$$

with $\alpha, \beta > 0$, and

$$z(q) = \frac{q - q_{\min}}{q_{\max} - q_{\min}}, \quad q_{\min} \leq q \leq q_{\max}. \quad (15)$$

Sometimes we shorten $z(q)$ to z . Since $I_{1,1}(z) = z$, we recover the conventional RED model [5] for $\alpha = \beta = 1$. The purpose of this generalization is to improve the stability properties by introducing the additional control parameters α and β . The beta distribution is related to the chi-square distribution [17]. By definition, $I_{\alpha,\beta}(x)$ is strictly increasing, hence invertible. Its inverse, $I_{\alpha,\beta}^{-1}(x)$, is also strictly increasing.

Thus, we consider hereafter a dynamical system,

$$q_{n+1} = f(q_n), \quad (16)$$

where the mapping $f : [0, B] \rightarrow [0, B]$ is defined as

$$f(q) = \begin{cases} (1-w)q + wB & \text{if } 0 \leq q \leq \theta_l, \\ (1-w)q + w \left(\frac{A_1}{\sqrt{I_{\alpha,\beta}(z(q))}} - A_2 \right) & \text{if } \theta_l < q < \theta_r, \\ (1-w)q & \text{if } \theta_r \leq q \leq B, \end{cases} \quad (17)$$

and the thresholds are given by

$$\theta_l = (q_{\max} - q_{\min}) I_{\alpha,\beta}^{-1}(p_1) + q_{\min}, \quad p_1 = \left(\frac{A_1}{A_2 + B} \right)^2, \quad (18)$$

where $p_1 < 1$ by (12), and

$$\theta_r = \begin{cases} (q_{\max} - q_{\min}) I_{\alpha,\beta}^{-1}(p_2) + q_{\min} & \text{if } p_2 = \left(\frac{A_1}{A_2} \right)^2 \leq 1, \\ q_{\max} & \text{otherwise,} \end{cases} \quad (19)$$

with

$$\begin{cases} \theta_r < q_{\max} & \text{if } 0 < A_1 < A_2, \\ \theta_r = q_{\max} & \text{if } A_2 \leq A_1 < A_2 + B, \end{cases} \quad (20)$$

and $\theta_l < \theta_r$ due to (12). Correspondingly,

$$0 < \frac{\theta_l - q_{\min}}{q_{\max} - q_{\min}} = z(\theta_l) \leq z(q) \leq z(\theta_r) = \frac{\theta_r - q_{\min}}{q_{\max} - q_{\min}} \leq 1, \quad \theta_l \leq q \leq \theta_r. \quad (21)$$

The thresholds θ_l and θ_r are set so that f is continuous on $[0, B]$, except when $A_1 > A_2$, in which case f is lower semicontinuous at θ_r . Indeed, if $A_1 > A_2$, then

$$\begin{aligned} f(\theta_r-) &= f(q_{\max}-) = \lim_{q \rightarrow q_{\max}-} f(q) = (1-w)q_{\max} + w(A_1 - A_2) = f(q_{\max}) + w(A_1 - A_2) \\ &> f(q_{\max}) = f(\theta_r), \end{aligned} \quad (22)$$

where we used $I_{\alpha,\beta}(z(q_{\max})) = I_{\alpha,\beta}(1) = 1$ on the first line of (22). To handle continuity ($A_1 \leq A_2$) and discontinuity ($A_1 > A_2$) at θ_r together, we use the notation $(A_1 - A_2)^+ = \max\{A_1 - A_2, 0\}$ (the positive part of $A_1 - A_2$) and write

$$f(\theta_r-) = f(\theta_r) + w(A_1 - A_2)^+ = \begin{cases} (1-w)\theta_r & \text{if } A_1 < A_2, \\ (1-w)q_{\max} & \text{if } A_1 = A_2, \\ (1-w)q_{\max} + w(A_1 - A_2) & \text{if } A_1 > A_2. \end{cases} \quad (23)$$

For further reference,

$$f(\theta_l) = (1-w)\theta_l + wB > \theta_l \quad (24)$$

$$f(\theta_r) = (1-w)\theta_r < \theta_r \quad (25)$$

and, in case $A_1 > A_2$,

$$f(q_{\max}-) < q_{\max} \Leftrightarrow A_1 - A_2 < q_{\max}. \quad (26)$$

Proposition 2 *It holds*

$$f(\theta_l) \geq f(\theta_r-) \Leftrightarrow w \geq \frac{\theta_r - \theta_l}{\theta_r - \theta_l + B - (A_1 - A_2)^+}. \quad (27)$$

Altogether, the (generalized) RED model has 6 system parameters (N, K, C, d, M, B) and 6 user parameters ($p_{\max}, q_{\min}, q_{\max}, w, \alpha, \beta$). The latter are also called control parameters because they can be tuned at will to stabilize the dynamic if necessary. It is worth noting that p_{\max} and the system parameters except B always appear grouped in the constants $A_1 = NK/\sqrt{p_{\max}}$ and $A_2 = Cd/M$. For mathematical simplicity, B could be set equal to 1 by taking normalized queue sizes q/B and also dividing A_1 and A_2 by B , but we will not. Although the mapping f depends explicitly on all those parameters, no subscripts have been appended to it for notational economy.

Figure 2 shows f for the system parameters

$$N = 1850, \quad C = 321,000 \text{ kbps}, \quad d = 0.012 \text{ s}, \quad K = 1.225, \quad M = 1 \text{ kB}, \quad B = 2000 \text{ packets}, \quad (28)$$

fixed control parameters

$$q_{\min} = 500, \quad q_{\max} = 1500, \quad w = 0.15, \quad (29)$$

and several choices for the remaining control parameters α, β and p_{\max} . The data (28) correspond to the Miguel Hernández University network; further information is given in Section 9.3.

4 Basic properties

In this section we study the properties of the first and second derivatives of f that will be needed below. Derivation of (17) yields

$$f'(q) = \begin{cases} 1-w & \text{if } 0 \leq q \leq \theta_l, \\ 1-w \left(1 + \frac{\nu A_1}{2} I_{\alpha,\beta}(z(q))^{-3/2} I'_{\alpha,\beta}(z(q)) \right) & \text{if } \theta_l < q < \theta_r, \\ 1-w & \text{if } \theta_r \leq q \leq B, \end{cases} \quad (30)$$

where one-sided derivatives (f'_+ and/or f'_-) are meant at endpoints and thresholds, and (see (15))

$$\nu = z'(q) = \frac{1}{q_{\max} - q_{\min}}, \quad (31)$$

$$I'_{\alpha,\beta}(x) = \frac{x^{\alpha-1}(1-x)^{\beta-1}}{\mathfrak{B}(1; \alpha, \beta)}. \quad (32)$$

Hence,

$$f'(q) < 1-w \text{ for all } q \in (\theta_l, \theta_r). \quad (33)$$

since $I_{\alpha,\beta}(z) > 0$ and $I'_{\alpha,\beta}(z) \geq 0$ for $z(\theta_l) \leq z \leq z(\theta_r)$. By continuity at θ_l ,

$$\begin{aligned} f'_+(\theta_l) &= f'(\theta_l+) = 1-w \left(1 + \frac{\nu A_1}{2} I_{\alpha,\beta}(z(\theta_l))^{-3/2} I'_{\alpha,\beta}(z(\theta_l)) \right) \\ &< 1-w = f'_-(\theta_l) \end{aligned} \quad (34)$$

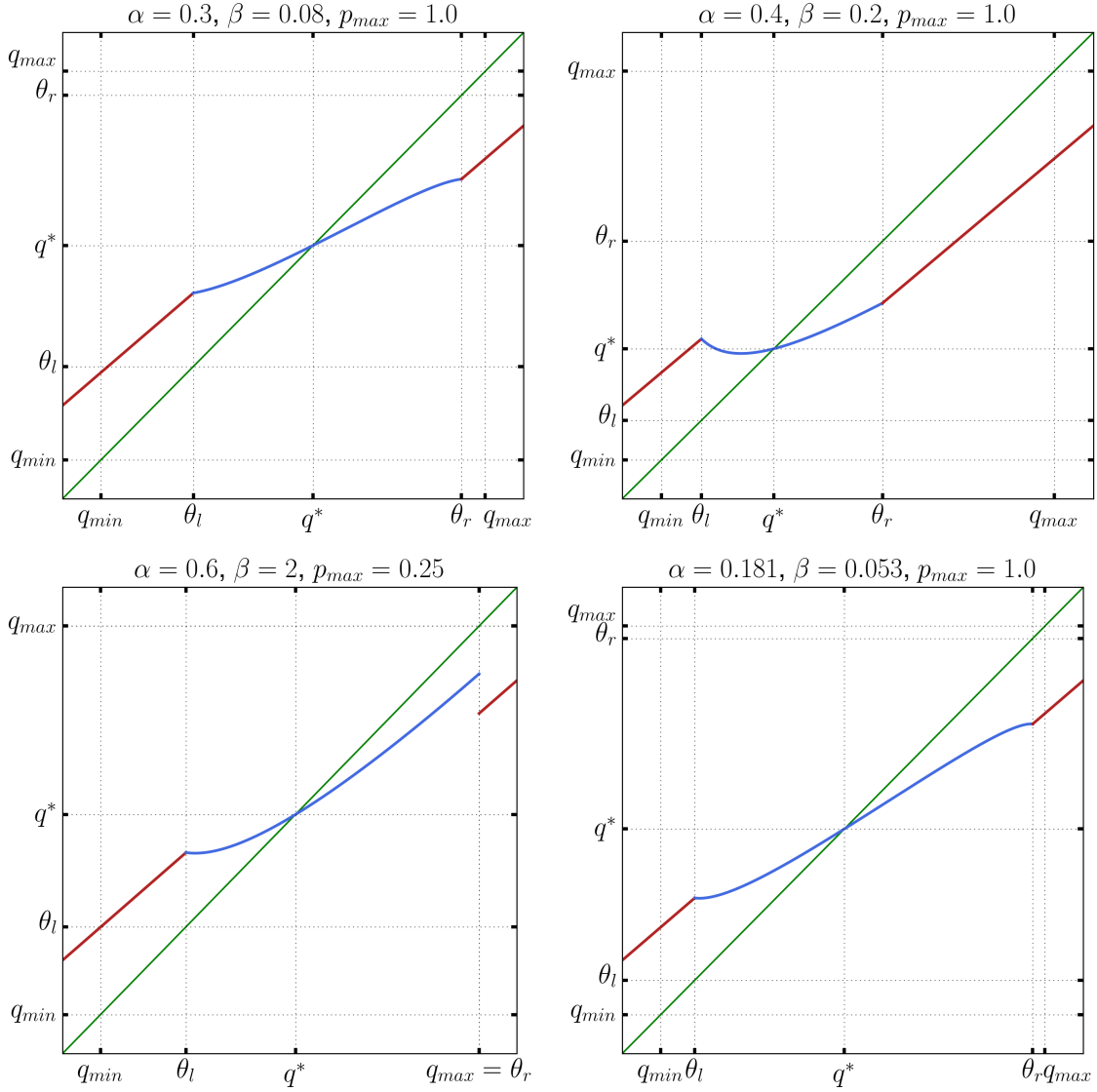


Figure 2: Graphs of the mapping f for the parameter settings (28), (29), and α, β and p_{max} as given on the top of each panel: monotonic increasing (top left), unimodal continuous (top right), unimodal discontinuous (bottom left), and bimodal (bottom right). $A_1 = 2265.8, A_2 = 3852.0$, except for the discontinuous graph, in which case $A_1 = 4531.6$ ($p_{max} = 0.25$). The point q^* (the fixed point of f , Section 5) is shown for further reference.

while

$$f'(\theta_r-) = \begin{cases} 1 - w \left(1 + \frac{\nu A_1}{2} I_{\alpha,\beta}(z(\theta_r))^{-3/2} I'_{\alpha,\beta}(z(\theta_r)) \right) < 1 - w = f'_+(\theta_r) & \text{if } A_1 < A_2, \\ f'(q_{\max-}) = 1 - w = f'_+(q_{\max}) & \text{if } A_1 \geq A_2, \beta \geq 1, \\ f'(q_{\max-}) = -\infty & \text{if } A_1 \geq A_2, \beta < 1, \end{cases} \quad (35)$$

since, by (32), $I'_{\alpha,\beta}(z(q_{\max})) = I'_{\alpha,\beta}(1) = 0$ if $\beta \geq 1$ and $I'_{\alpha,\beta}(z(q_{\max})) = I'_{\alpha,\beta}(1) = \infty$ if $\beta < 1$.

From (33), along with $f(\theta_l) = (1-w)\theta_l + wB$ and $f(\theta_r-) = (1-w)\theta_r + w(A_1 - A_2)^+$ (Equation (23)), we obtain:

Proposition 3 *The mapping f on (θ_l, θ_r) is bounded as follows:*

$$(1-w)q + w(A_1 - A_2)^+ < f(q) < (1-w)q + wB. \quad (36)$$

By (12), $A_1 - A_2 < B$. We call $q \mapsto (1-w)q + w(A_1 - A_2)^+$ and $q \mapsto (1-w)q + wB$ the lower and upper envelopes of f on (θ_l, θ_r) , respectively.

Derivation of (30) yields

$$f''(q) = \frac{w\nu^2 A_1}{2} I_{\alpha,\beta}(z)^{-3/2} \left(\frac{3}{2} I_{\alpha,\beta}(z)^{-1} I'_{\alpha,\beta}(z)^2 - I''_{\alpha,\beta}(z) \right) \quad (37)$$

for $\theta_l < q < \theta_r$, and $f''(q) = 0$ otherwise. Since

$$I''_{\alpha,\beta}(z) = I'_{\alpha,\beta}(z) h_{\alpha,\beta}(z), \quad \text{with } h_{\alpha,\beta}(z) := \frac{\alpha - 1}{z} - \frac{\beta - 1}{1 - z}, \quad (38)$$

Equation (37) can be written in a more convenient way as

$$f''|_{(\theta_l, \theta_r)}(q) = \frac{w\nu^2 A_1}{4} I_{\alpha,\beta}(z)^{-3/2} I'_{\alpha,\beta}(z) [3J_{\alpha,\beta}(z) - 2h_{\alpha,\beta}(z)], \quad (39)$$

where $f|_{(\theta_l, \theta_r)} : (\theta_l, \theta_r) \rightarrow (\theta_l, \theta_r)$ denotes as usual the restriction of f to the interval (θ_l, θ_r) ,

$$f|_{(\theta_l, \theta_r)}(q) = (1-w)q + w \left(A_1 I_{\alpha,\beta}(z(q))^{-1/2} - A_2 \right), \quad (40)$$

and

$$J_{\alpha,\beta}(z) := \frac{I'_{\alpha,\beta}(z)}{I_{\alpha,\beta}(z)} > 0 \quad (41)$$

for all $z(\theta_l) < z < z(\theta_r)$ (see (21)).

Proposition 4 *Suppose that $3J_{\alpha,\beta}(z(q)) - 2h_{\alpha,\beta}(z(q)) > 0$ for $\theta_l < q < \theta_r$. It holds:*

- (a) $f|_{(\theta_l, \theta_r)}$ is \cup -convex.
- (b) If $f'(\theta_l+) \cdot f'(\theta_r-) > 0$, then $f|_{(\theta_l, \theta_r)}$ has no critical point. Otherwise, if $f'(\theta_l+) \cdot f'(\theta_r-) < 0$, then $f|_{(\theta_l, \theta_r)}$ has one critical point.

Proof. The assumption implies $f''|_{(\theta_l, \theta_r)}(q) > 0$ by (39). In such a case, $f'|_{(\theta_l, \theta_r)}$ is increasing, so that $f|_{(\theta_l, \theta_r)}$ is a \cup -convex mapping with one critical point if $f'|_{(\theta_l, \theta_r)}$ takes both signs, or no critical point otherwise. ■

Proposition 5 *$f''|_{(\theta_l, \theta_r)}$ cannot vanish identically on an open set.*

Proof. The case $\alpha = \beta = 1$ is trivial. Otherwise,

$$J_{\alpha,\beta}(z) = \frac{I'_{\alpha,\beta}(z)}{I_{\alpha,\beta}(z)} = \frac{d}{dz} \ln I_{\alpha,\beta}(z), \quad h_{\alpha,\beta}(z) = \frac{I''_{\alpha,\beta}(z)}{I'_{\alpha,\beta}(z)} = \frac{d}{dz} \ln I'_{\alpha,\beta}(z),$$

so $3I_{\alpha,\beta}(z)^{-1} I'_{\alpha,\beta}(z) = 2h_{\alpha,\beta}(z)$ on an open set $O \subset (\nu\theta_l - q_{\min}, \nu\theta_r - q_{\min})$ implies $I_{\alpha,\beta}(z)^{3/2} = \text{const} \cdot I'_{\alpha,\beta}(z)$ on O . By analyticity, this identity extends from O to $(0, 1)$. But $I_{\alpha,\beta}(z)^{3/2}$ is strictly increasing on $(0, 1)$ and is well-defined at $z = 0, 1$, whereas, depending on α and β , $I'_{\alpha,\beta}(z)$ has a critical point in $(0, 1)$, or diverges at $z = 0$, or diverges at $z = 1$ —a contradiction. ■

The first and second derivatives of $f(q)$, $q \neq \theta_l, \theta_r$, are related as follows. By (30),

$$I_{\alpha,\beta}(z(q))^{-3/2} I'_{\alpha,\beta}(z(q)) = \frac{2}{w\nu A_1} (1 - w - f'(q)) \quad (42)$$

for every $q \in (\theta_l, \theta_r)$. Plug this into (39) to obtain

$$f''(q) = \frac{\nu}{2} (1 - w - f'(q)) [3J_{\alpha,\beta}(z(q)) - 2h_{\alpha,\beta}(z(q))], \quad (43)$$

both for $q \in (\theta_l, \theta_r)$ and $q \in [0, \theta_l) \cup (\theta_r, B]$ since $f'(q) = 1 - w$ in the latter case. In particular, if q_c is a critical point ($f'(q_c) = 0$ implies $q_c \in (\theta_l, \theta_r)$), then

$$f''(q_c) = \frac{(1-w)\nu}{2} [3J_{\alpha,\beta}(z(q_c)) - 2h_{\alpha,\beta}(z(q_c))], \quad (44)$$

where $J_{\alpha,\beta}(z(q_c)) = \frac{2(1-w)}{w\nu A_1} I_{\alpha,\beta}(z(q_c))^{1/2}$ by (42).

5 Local stability

We begin by studying the fixed points of f .

Theorem 6 *The mapping f has a unique fixed point $q^* \in (\theta_l, \theta_r)$ if and only if $A_1 < A_2 + q_{\max}$; otherwise, it has none. Furthermore, q^* does not depend on w .*

Proof. By definition, the graph of f lies strictly above the bisector on $[0, \theta_l]$, while it lies strictly below the bisector on $[\theta_r, B]$. Suppose, furthermore, that $A_1 \leq A_2$ so that f is continuous on $[\theta_l, \theta_r]$ with $f(\theta_l) > \theta_l$ (see (24)) and $f(\theta_r) < \theta_r$ (see (25)). By continuity, there is a point $q^* \in (\theta_l, \theta_r)$ at which the graph of $f(q)$ crosses the bisector, i.e., $f(q^*) = q^*$. This point is unique because

$$f(q) = q \Leftrightarrow \frac{A_1}{\sqrt{I_{\alpha,\beta}(z(q))}} = q + A_2 \quad (45)$$

($\theta_l < q < \theta_r$), where $q \mapsto A_1/\sqrt{I_{\alpha,\beta}(z(q))}$ is a strictly decreasing function and $q \mapsto q + A_2$ is a strictly increasing function.

To deal with the case $A_1 > A_2$, apply (26), i.e., $f(\theta_r -) = f(q_{\max} -) < q_{\max}$ if and only if $A_1 < A_2 + q_{\max}$. Define then $g = f$ on $[\theta_l, q_{\max})$ and $g(q_{\max}) = f(q_{\max} -)$, so that g is continuous on $[\theta_l, q_{\max}]$ with $g(\theta_l) > \theta_l$ and $g(q_{\max}) < q_{\max}$. As before, we conclude that g has a unique fixed point $q^* \in (\theta_l, q_{\max})$. The same must hold for f because $f = g$ on $[\theta_l, q_{\max})$ and $f(q_{\max}) = (1-w)q_{\max} < q_{\max}$.

If $A_1 = A_2 + q_{\max}$, then $f(q_{\max} -) = q_{\max}$, i.e., q_{\max} is the fixed point of g , the continuous extension of $f|_{[\theta_l, q_{\max})}$ to $[\theta_l, q_{\max}]$. More generally, if $A_1 \geq A_2 + q_{\max}$, then $f(q_{\max} -) \geq q_{\max}$. As a result, f has no fixed point (neither on (θ_l, θ_r) nor, of course, on $[0, B]$). ■

In other words, the RED dynamics (16)-(17) has a unique stationary or equilibrium state q^* , as long as $A_1 < A_2 + q_{\max}$. The dependence of q^* on the system parameters and p_{\max} occurs through the constants A_1 and A_2 , Equation (9). See Figure 2 for q^* with different settings of α , β and A_1 . To compute q^* one has to solve numerically the equation (45). Note from (45) that

$$A_1 = (q^* + A_2) \sqrt{I_{\alpha,\beta}(z^*)}, \quad (46)$$

where $z^* = z(q^*) = \nu(q^* - q_{\min})$.

Remark 7 *According to Theorem 6, f has no fixed points if $A_1 \geq A_2 + q_{\max}$, so this possibility will be no longer considered.*

A sufficient condition for the fixed point q^* to be attractive is $|f'(q^*)| < 1$. Otherwise, if $|f'(q^*)| > 1$, q^* is a repeller. If $|f'(q^*)| = 1$, then q^* can be attracting, repelling, semistable, or even none of these.

In our case, $f'(q^*) < 1 - w$ by Equation (33), so for the local stability of the RED dynamics at q^* it suffices actually that $f'(q^*) > -1$, i.e.,

$$w \left(1 + \frac{\nu A_1}{2} I_{\alpha,\beta}(z^*)^{-3/2} I'_{\alpha,\beta}(z^*) \right) < 2. \quad (47)$$

Intuitively speaking, a bifurcation occurs when a small change in a parameter causes a qualitative change in the dynamic. Since we are only interested in the stability of q^* , we will call *bifurcation point* a parameter value at which q^* loses stability. If this happens for increasing (resp. decreasing) values of the parameter, we speak of a direct (resp. reverse) bifurcation. Therefore, bifurcation points verify the condition $f'(q^*) = -1$, that is,

$$w \left(1 + \frac{\nu A_1}{2} I_{\alpha,\beta}(z^*)^{-3/2} I'_{\alpha,\beta}(z^*) \right) = 2. \quad (48)$$

In particular, from (48) we obtain that

$$w_{\text{bif}} = \frac{2}{1 + \frac{\nu A_1}{2} I_{\alpha,\beta}(z^*)^{-3/2} I'_{\alpha,\beta}(z^*)} \quad (49)$$

is the bifurcation point of the averaging weight. Plugging (46) into (49) we obtain the alternative expression

$$w_{\text{bif}} = \frac{2}{1 + \frac{\nu}{2}(q^* + A_2) I_{\alpha,\beta}(z^*)^{-1/2} I'_{\alpha,\beta}(z^*)}. \quad (50)$$

In either case, for each α, β there is a continuum of different choices of parameters, lying on the level surfaces $NK/\sqrt{p_{\max}} = A_1$ and $Cd/M = A_2$ in the corresponding 3-dimensional parametric spaces, that give the same bifurcation point w_{bif} .

Similarly,

$$A_{1,\text{bif}} = \frac{4 - 2w}{\nu w I_{\alpha,\beta}(z^*)^{-3/2} I'_{\alpha,\beta}(z^*)} \quad (51)$$

and (see (46))

$$A_{2,\text{bif}} = \frac{4 - 2w}{\nu w I_{\alpha,\beta}(z^*)^{-1} I'_{\alpha,\beta}(z^*)} - q^*, \quad (52)$$

where, according to Theorem 6 and (46), q^* (and z^*) depend, in turn, on $A_{1,\text{bif}}$ or $A_{2,\text{bif}}$, respectively. Both formulas can be used to calculate numerically $A_{1,\text{bif}}$ (resp. $A_{2,\text{bif}}$), provided the discrepancy $|A_1 - A_{1,\text{bif}}|$ (resp. $|A_2 - A_{2,\text{bif}}|$) approaches 0 as the computation loop $A_1 \rightarrow q^* \rightarrow A_{1,\text{bif}}$ (resp. $A_2 \rightarrow q^* \rightarrow A_{2,\text{bif}}$) is repeated. For each α, β , the bifurcation points of N , K , and p_{\max} (resp. C , d , M) lie on the level surface $NK/\sqrt{p_{\max}} = A_{1,\text{bif}}$ (resp. $Cd/M = A_{2,\text{bif}}$).

6 Examples

We consider here a few settings of α and β leading to models amenable to analytic calculations.

Example 8 For $\beta = 1$,

$$I_{\alpha,1}(x) = x^\alpha, \quad I'_{\alpha,1}(x) = \alpha x^{\alpha-1}, \quad I_{\alpha,1}^{-1}(y) = y^{1/\alpha},$$

thus,

$$\begin{aligned} f|_{(\theta_l, \theta_r)}(q) &= (1-w)q + w \left(\frac{A_1}{z^{\alpha/2}} - A_2 \right), \\ f'|_{(\theta_l, \theta_r)}(q) &= 1 - w \left(1 + \frac{\alpha \nu A_1}{2 z^{\alpha/2+1}} \right). \end{aligned}$$

Since $q \mapsto q^{\alpha/2+1}$ is an increasing function for $\alpha > 0$, it follows that $f'|_{(\theta_l, \theta_r)}$ is also an increasing function, hence $f|_{(\theta_l, \theta_r)}$ is \cup -convex. Indeed,

$$f''|_{(\theta_l, \theta_r)}(q) = \frac{\alpha(\alpha+2)\nu^2 w A_1}{4 z^{\alpha/2+2}} > 0 \quad (53)$$

for all $\alpha > 0$. Therefore, $f|_{(\theta_l, \theta_r)}$ has one critical point q_c if $f'|_{(\theta_l, \theta_r)}$ takes both signs and none otherwise. Moreover,

$$f'|_{(\theta_l, \theta_r)}(q_c) = 0 \Leftrightarrow z_c := z(q_c) = \left(\frac{\alpha \nu w A_1}{2(1-w)} \right)^{\frac{2}{\alpha+2}}, \quad (54)$$

provided

$$\nu(\theta_l - q_{\min}) < z_c < \nu(\theta_r - q_{\min}), \quad (55)$$

in which case $f|_{(\theta_l, \theta_r)}$ has a global minimum at

$$q_c = \frac{z_c}{\nu} + q_{\min} = (q_{\max} - q_{\min})z_c + q_{\min}.$$

Otherwise, $f|_{(\theta_l, \theta_r)}$ has no critical point. By (45), the fixed point is given by $q^* = z^*/\nu + q_{\min}$, where z^* is the solution of the equation

$$z^{\alpha/2+1} + \nu(A_2 + q_{\min})z^{\alpha/2} - \nu A_1 = 0, \quad (56)$$

and, by (49), a bifurcation of the dynamics occurs at the point

$$w_{\text{bif}} = \frac{4z^{*\alpha/2+1}}{2z^{*\alpha/2+1} + \alpha\nu A_1} \quad (57)$$

when all other parameters in (57) are kept constant. Note that if $A_1 = A_2 + q_{\max}$, then $A_2 + q_{\min} = A_1 - \frac{1}{\nu}$, so $z^* = 1$ is a solution of (56), i.e., $f(q_{\max}^-) = q_{\max}$ in such a case (see the proof of Theorem 6).

Example 9 To obtain the original RED model [5], set $\alpha = 1$ in Example 8. Thus, Equation (54) reads

$$z_c = \left(\frac{\nu w A_1}{2(1-w)} \right)^{\frac{2}{3}}$$

and Equation (56) for z^* becomes

$$z^{3/2} + \nu(A_2 + q_{\min})z^{1/2} - \nu A_1 = 0,$$

a cubic equation for $z^{1/2}$. The only real root of this equation is given by

$$z^{*1/2} = -2\sqrt{\frac{\nu(A_2 + q_{\min})}{3}} \sinh \left(\frac{1}{3} \sinh^{-1} \left(-\frac{3A_1}{2(A_2 + q_{\min})} \sqrt{\frac{3}{\nu(A_2 + q_{\min})}} \right) \right).$$

Once $z^{*1/2}$ has been computed, we can compute w_{bif} via (57),

$$w_{\text{bif}} = \frac{4z^{*1/2+1}}{2z^{*1/2+1} + \nu A_1}.$$

Example 10 Finally, consider the model with $\alpha = 2$, $\beta = 1$. Equation (54) reads then

$$z_c = \left(\frac{\nu w A_1}{1-w} \right)^{\frac{1}{2}},$$

Equation (56) becomes

$$z^2 + \nu(A_2 + q_{\min})z - \nu A_1 = 0$$

which positive solution is

$$z^* = \frac{\nu}{2} \left(\sqrt{(A_2 + q_{\min})^2 + 4A_1/\nu} - (A_2 + q_{\min}) \right),$$

and Equation (57) turns to

$$w_{\text{bif}} = \frac{2z^{*2}}{z^{*2} + \nu A_1}.$$

7 Global stability

Let $\mathcal{B}(S, f)$ denote the basin of attraction of a set $S \subset [0, B]$, that is, $\mathcal{B}(S, f)$ consists of all points of $[0, B]$ that asymptotically end up in S .

Theorem 11 *If (θ_l, θ_r) is invariant, then $\mathcal{B}((\theta_l, \theta_r), f) = [0, B]$.*

Proof. (i) Suppose first that $A_1 \leq A_2$ so that f is continuous at θ_r .

(i-1) If $q_0 \in [0, \theta_l]$, then

$$q_{n+1} = f(q_n) = (1-w)q_n + wB = q_n + w(B - q_n) > q_n$$

as long as $q_n \in [0, \theta_l]$. Therefore, since there is no fixed point of f in $[0, \theta_l]$, the orbit of q_0 leaves $[0, \theta_l]$ through the right side. Suppose that $q_{n_0}, n_0 \geq 1$, is the first point of the orbit of q_0 such that $q_{n_0} > \theta_l$. Then $q_{n_0-1} \leq \theta_l$ and the increasing monotonicity of f on $[0, \theta_l]$ implies $q_{n_0} = f(q_{n_0-1}) \leq f(\theta_l) \leq \theta_r$, the latter inequality following from the continuity of f at θ_l and the invariance of (θ_l, θ_r) . So, $q_{n_0} \in (\theta_l, \theta_r)$ unless $q_{n_0-1} = \theta_l$ and $q_{n_0} = f(\theta_l) = \theta_r$.

(i-2) A similar argument applies when $q_0 \in [\theta_r, B]$, with the difference that the initial segment of the orbit of q_0 is strictly decreasing,

$$q_{n+1} = f(q_n) = (1-w)q_n < q_n,$$

as long as $q_n \in [\theta_r, B]$, and $q_{n_0-1} \geq \theta_r$ (q_{n_0} being the first point of the orbit of q_0 such that $q_{n_0} < \theta_r$) implies $q_{n_0} = f(q_{n_0-1}) \geq f(\theta_r) \geq \theta_l$, the latter inequality following from the continuity of f at θ_r and the invariance of (θ_l, θ_r) . In this case $q_{n_0} \in (\theta_l, \theta_r)$ unless $q_{n_0-1} = \theta_r$ and $q_{n_0} = f(\theta_r) = \theta_l$.

(ii) Suppose now that $A_1 > A_2$ so that f is discontinuous at $\theta_r = q_{\max}$.

(ii-1) If $q_0 \in [0, \theta_l]$ nothing changes in the above argument in case (i-1) since f is continuous at θ_l .

(ii-2) If $q_0 \in [\theta_r, B]$ and $q_{n_0}, n_0 \geq 1$, is the first point of the orbit of q_0 such that $q_{n_0} \leq \theta_r$, then $q_{n_0-1} \geq \theta_r$ and the increasing monotonicity of f on $[\theta_r, B]$ implies $q_{n_0} = f(q_{n_0-1}) \geq f(\theta_r)$. This time we cannot argue, as in case (i-2), that $f(\theta_r) \geq \theta_l$ to conclude $q_{n_0} \geq \theta_l$ because f is not continuous at θ_r . However, if $q_{n_0} < \theta_l$ then we are in case (ii-1). Hence, there is $n_1 > n_0$ such that $q_{n_1} \in (\theta_l, \theta_r)$ unless $q_{n_1-1} = \theta_l$ and $q_{n_1} = f(\theta_l) = \theta_r$. ■

We conclude from Theorem 11 that the interesting dynamics takes place in the interval $[\theta_l, \theta_r]$ or, in more technical terms, $[\theta_l, \theta_r]$ contains the non-wandering set for f . It follows from the proof of Theorem 11 that the only way to prevent the orbit of $q_0 \in [0, \theta_l] \cup [\theta_r, B]$ from getting trapped within (θ_l, θ_r) is that it is a preimage of an hypothetical periodic cycle $f(\theta_l) = \theta_r$ and $f(\theta_r) = \theta_l$. We show next that $\theta_l + \theta_r \neq B$ excludes the latter possibility.

Proposition 12 *If $f(\theta_l) = \theta_r$ and $f(\theta_r) = \theta_l$ (i.e., $\{\theta_l, \theta_r\}$ is a periodic orbit of period 2), then $\theta_l + \theta_r = B$. If furthermore, $[\theta_l, \theta_r]$ is invariant, then $f([\theta_l, \theta_r]) = [\theta_l, \theta_r]$.*

Proof. $f(\theta_l) = (1-w)\theta_l + wB = \theta_r$ implies $w = (\theta_r - \theta_l)/(B - \theta_l)$, while $f(\theta_r) = (1-w)\theta_r = \theta_l$ implies $w = (\theta_r - \theta_l)/\theta_r$, so $B - \theta_l = \theta_r$ when both conditions hold simultaneously. The second statement is obvious. ■

If $\mathcal{B}(q^*, f) = [0, B]$ we say that q^* is a global attractor of f , what amounts to q^* being globally stable. Equivalently, we say also that f is globally stable. The following theorem, which combines the results of Theorems 6 and 11, and Proposition 12, tells us how to further proceed regarding this issue.

Theorem 13 *Let $q^* \in (\theta_l, \theta_r)$ be the unique fixed point of f (hence, $A_1 < A_2 + q_{\max}$). If*

- (i) (θ_l, θ_r) is invariant (so that $f|_{(\theta_l, \theta_r)}$ defines a dynamical system on (θ_l, θ_r)),
- (ii) $\theta_l + \theta_r \neq B$ (so that $\{\theta_l, \theta_r\}$ is not a periodic orbit), and
- (iii) $\mathcal{B}(q^*, f|_{(\theta_l, \theta_r)}) = (\theta_l, \theta_r)$ (i.e., q^* is a global attractor of $f|_{(\theta_l, \theta_r)}$)

then q^* is a global attractor of f .

Therefore, when it comes to study the global stability of the RED dynamics it suffices to focus on $f|_{(\theta_l, \theta_r)}$, as long as $A_1 < A_2 + q_{\max}$, and conditions (i) and (ii) in Theorem 13 are fulfilled.

The results in Section 4 and numerical calculations show that $f|_{(\theta_l, \theta_r)}$ can have none or several local extrema, depending on the parameter configuration; see Figure 2. Since our objective is to design an adaptive and simple congestion control, we consider in the next two subsections the following special cases: $f|_{(\theta_l, \theta_r)}$ is monotonic (Section 7.1), and $f|_{(\theta_l, \theta_r)}$ is unimodal, i.e., there exists $q_c \in (\theta_l, \theta_r)$ such that f has opposite monotonicity on $(\theta_l, q_c]$ and $[q_c, \theta_r)$ (Section 7.2); q_c is called a turning point and $f'(q_c) = 0$. By Proposition 5, $f|_{(\theta_l, \theta_r)}$ is always strictly monotonic on each monotonicity segment (though not always explicitly stated).

7.1 Monotonic case

In this case, $f|_{(\theta_l, \theta_r)}$ is (strictly) increasing if and only if $f(\theta_l) = f(\theta_l+) < f(\theta_r-)$, or (strictly) decreasing if and only if $f(\theta_l) = f(\theta_l+) > f(\theta_r-)$, where $f(\theta_r-)$ is given in (23). By Proposition 2,

$$f|_{(\theta_l, \theta_r)} \text{ is increasing} \Leftrightarrow w < \frac{\theta_r - \theta_l}{\theta_r - \theta_l + B - (A_1 - A_2)^+} =: w_{\text{mon}} \quad (58)$$

where $\theta_r = q_{\max}$ if $A_1 \geq A_2$, and

$$f|_{(\theta_l, \theta_r)} \text{ is decreasing} \Leftrightarrow w > w_{\text{mon}}. \quad (59)$$

Proposition 14 (a) Suppose that $f|_{(\theta_l, \theta_r)}$ is increasing. Then (θ_l, θ_r) is invariant if and only if $(A_1 - A_2)^+ < q_{\max}$.

(b) Suppose that $f|_{(\theta_l, \theta_r)}$ is decreasing. Then (θ_l, θ_r) is invariant if and only if

$$w \leq \min \left\{ \frac{\theta_r - \theta_l}{B - \theta_l}, \frac{\theta_r - \theta_l}{\theta_r - (A_1 - A_2)^+} \right\} =: w_{\text{inv}}, \quad (60)$$

where $\theta_r = q_{\max}$ if $(A_1 - A_2)^+ > 0$ (Equation 20).

Proof. Since $f|_{(\theta_l, \theta_r)}$ is strictly monotonic, we need to consider only the boundary points θ_l and θ_r . Remember that $f(\theta_l) > \theta_l$ by (24) and $f(\theta_r) < \theta_r$ in the continuous case ($A_1 \leq A_2$) by (25), but, in the discontinuous case ($A_1 > A_2$), $f(q_{\max-}) < q_{\max}$ if and only if $(A_1 - A_2)^+ < q_{\max}$ by (26).

(a) Suppose that $f|_{(\theta_l, \theta_r)}$ is increasing. If $A_1 \leq A_2$, then

$$(\theta_l, \theta_r) \text{ is invariant} \Leftrightarrow \begin{cases} \text{(i)} f(\theta_l) < \theta_r, \\ \text{(ii)} f(\theta_r) > \theta_l. \end{cases}$$

Conditions (i)-(ii) hold because $\theta_l < f(\theta_l) < f(\theta_r) < \theta_r$, where the second inequality follows from the strictly increasing monotonicity of $f|_{(\theta_l, \theta_r)}$. Thus, (θ_l, θ_r) is automatically invariant; note that the condition $(A_1 - A_2)^+ < q_{\max}$ in the formulation of Proposition 14(a) boils down in this particular case to $q_{\max} > 0$, which indeed imposes no restriction whatsoever.

Otherwise, if $A_1 > A_2$ (hence $\theta_r = q_{\max}$), then

$$(\theta_l, q_{\max}) \text{ is invariant} \Leftrightarrow \begin{cases} \text{(i)} f(\theta_l) < q_{\max}, \\ \text{(ii)} f(q_{\max-}) < q_{\max}, \\ \text{(iii)} f(q_{\max-}) > \theta_l. \end{cases}$$

Conditions (i)-(iii) hold because $\theta_l < f(\theta_l) < f(q_{\max-}) < q_{\max}$, where the second inequality follows again from the strictly increasing monotonicity of $f|_{(\theta_l, q_{\max})}$, and the third one holds if and only if $(A_1 - A_2)^+ < q_{\max}$ by (26).

(b) Suppose now that $f|_{(\theta_l, \theta_r)}$ is decreasing. If $A_1 \leq A_2$, then

$$(\theta_l, \theta_r) \text{ is invariant} \Leftrightarrow \begin{cases} \text{(i)} f(\theta_l) < \theta_r & \Leftrightarrow w \leq (\theta_r - \theta_l)/(B - \theta_l), \\ \text{(ii)} f(\theta_r) > \theta_l & \Leftrightarrow w \leq (\theta_r - \theta_l)/\theta_r. \end{cases}$$

Otherwise, if $A_1 > A_2$, then

$$(\theta_l, \theta_r) \text{ is invariant} \Leftrightarrow \begin{cases} \text{(i)} f(\theta_l) < q_{\max} & \Leftrightarrow w \leq (q_{\max} - \theta_l)/(B - \theta_l), \\ \text{(ii)} f(q_{\max-}) < q_{\max}, \\ \text{(iii)} f(q_{\max-}) > \theta_l. & \Leftrightarrow w \leq (q_{\max} - \theta_l)/(q_{\max} - (A_1 - A_2)^+). \end{cases}$$

Condition (ii) holds because $f(q_{\max-}) < f(\theta_l)$ by the strictly decreasing monotonicity of $f|_{(\theta_l, q_{\max})}$. Thus, if $w \leq \frac{q_{\max} - \theta_l}{B - \theta_l}$, then $f(q_{\max-}) < q_{\max}$ by (i). Moreover, $f(q_{\max-}) < q_{\max}$ if and only if $(A_1 - A_2)^+ < q_{\max}$ by (26), so that the bound $\frac{q_{\max} - \theta_l}{q_{\max} - (A_1 - A_2)^+}$ in (iii) is positive. The latter statement follows also from $w > w_{\text{mon}} > 0$ for a decreasing $f|_{(\theta_l, q_{\max})}$, Equation (59). ■

Remark 15 It follows from Proposition 14(a) and Theorem 6 that an increasing $f|_{(\theta_l, \theta_r)}$ with $A_1 = A_2 + q_{\max}$ has an invariant interval $(\theta_l, \theta_r) = (\theta_l, q_{\max})$ but no fixed point; indeed, in this case $q^* = q_{\max} \notin (\theta_l, q_{\max})$. Furthermore, comparison of (59) and (60) shows that if $(A_1 - A_2)^+ < \theta_r$ (which actually means $(A_1 - A_2)^+ < q_{\max}$ by (20)), then

$$w_{\text{mon}} < \frac{\theta_r - \theta_l}{B - \theta_l} \text{ and } w_{\text{mon}} < \frac{\theta_r - \theta_l}{\theta_r - (A_1 - A_2)^+},$$

hence

$$0 < w_{\text{mon}} < w_{\text{inv}} < 1. \quad (61)$$

This confirms that an invariant interval (θ_l, θ_r) can accommodate both increasing and decreasing mappings with a fixed point.

The study of the global attraction of increasing mappings is rather simple, as we will see in the next theorem. Decreasing mappings are more difficult to handle because of the possible existence of periodic orbits of period 2 (2-cycles for short). Out of the different hypotheses that can prevent the existence of 2-cycles in (θ_l, θ_r) , we are going to resort to the perhaps simplest ones regarding the scope of this paper.

Theorem 16 (a) *If $f|_{(\theta_l, \theta_r)}$ is increasing and $A_1 < A_2 + q_{\max}$, then $\mathcal{B}(q^*, f|_{(\theta_l, \theta_r)}) = (\theta_l, \theta_r)$.*

(b) *If $f|_{(\theta_l, \theta_r)}$ is decreasing with $f'|_{(\theta_l, \theta_r)}(q) > -1$ and $w \leq w_{\text{inv}}$, then $\mathcal{B}(q^*, f|_{(\theta_l, \theta_r)}) = (\theta_l, \theta_r)$.*

Proof. (a) Suppose that f is increasing on (θ_l, θ_r) . Since $A_1 < A_2 + q_{\max}$, the interval (θ_l, θ_r) is invariant by Proposition 14(i). For any $q_n = f^n(q_0)$, $n \geq 0$, it holds

$$\theta_l < q_n < q^* \Rightarrow q_n < f(q_n) < q^* \quad (62)$$

because $f(\theta_l) > \theta_l$, $f|_{(\theta_l, \theta_r)}$ is strictly increasing, and there is no fixed point other than q^* (thus, the graph of $f|_{(\theta_l, \theta_r)}$ lies above the bisector for $q < q^*$), and

$$q^* < q_n < \theta_r \Rightarrow q^* < f(q_n) < q_n \quad (63)$$

because $f(\theta_r) < \theta_r$, $f|_{(\theta_l, \theta_r)}$ is strictly increasing, and there is no fixed point other than q^* (thus, the graph of $f|_{(\theta_l, \theta_r)}$ lies below the bisector for $q > q^*$). Therefore, the orbits of all initial conditions $q_0 \in (\theta_l, \theta_r)$ converge to q^* .

(b) Suppose now that f is decreasing on (θ_l, θ_r) . Since $w \leq w_{\text{inv}}$, the interval (θ_l, θ_r) is invariant by Proposition 14(b). In this case, the second iterate $f^2 = f \circ f$ is increasing on (θ_l, θ_r) . Moreover, the condition $f'|_{(\theta_l, \theta_r)}(q) > -1$ warrants that f^2 has no fixed points in (θ_l, θ_r) other than q^* (otherwise, the derivative of $f^2(q) - q$ would vanish at some intermediate point between q^* and an endpoint). Apply now to f^2 the same argument as in the proof of (a). As a result, this time the convergence of the orbit points $f^n(q_0)$ to q^* is alternating, approaching the even iterates q^* from the same side where q_0 lies, and the odd iterates from the opposite side (since $f^{2n+1}(q_0) = f(f^{2n}(q_0))$ and f is decreasing). ■

Remark 17 *Note that no hypothesis was made in (a) regarding the magnitude of $f'|_{(\theta_l, \theta_r)}$ because the graph of $f|_{(\theta_l, \theta_r)}$ crosses transversally the bisector at q^* , so $f'(q^*) < 1$ and q^* is locally attracting. The restriction $f'|_{(\theta_l, \theta_r)}(q) > -1$ in (b) can be replaced by the absence of 2-cycles. According to Theorem 11, the existence of 2-cycles has to be also excluded at the endpoints $\{\theta_l, \theta_r\}$, should q^* be a global attractor. This can be done, as in Theorem 13, with the proviso $\theta_l + \theta_r \neq B$. By Sharkovsky's theorem [18] applied to the continuous case ($A_1 \leq A_2$), if there are no periodic orbits of period 2, then there are no periodic orbits of any period.*

Properties (62) and (63) are sometimes called negative feedback conditions and, as shown in the proof of Theorem 16, they are determinant in many proofs of local and global stability of fixed points in one-dimensional dynamics. Another useful tool is the Schwarzian derivative

$$Sf(q) = \frac{f'''(q)}{f'(q)} - \frac{3}{2} \left(\frac{f''(q)}{f'(q)} \right)^2, \quad (64)$$

particularly when f is a polynomial and all the roots of f' are real and simple. In view of (30) and (37), we anticipate that Sf will be of little help for our purposes. We will come back to this point in short.

7.2 Unimodal case

A mapping with k turning points is called unimodal if $k = 1$, multimodal if $k \geq 2$ or, generically, k -modal. In this case, the mapping is expected to be chaotic, meaning that the attractor is a union of intervals or, in a weaker sense, that there is an infinite number of periodic orbits [19]. For the kinds of attractors that can appear with unimodal maps, see e.g. [7, 6]. The growth rate of periodic orbits with the period is quantified by the topological entropy [20, 21, 22], while their stability is related to the sign of the Schwarzian derivative [23]. Global stability of multimodal mappings with a single, locally attractive fixed point can be only achieved if the map has no 2-cycles.

We consider in this section a RED dynamics in which $f|_{(\theta_l, \theta_r)}$ has only one local extremum (hence, a global extremum) at $q_c \in (\theta_l, \theta_r)$. Multimodal mappings are not interesting for our purposes.

Proposition 18 (a) *Suppose that $f(q_c)$ is a minimum. Then (θ_l, θ_r) is invariant if and only if*

$$w \leq \frac{\theta_r - \theta_l}{B - \theta_l}, \quad f(q_c) > \theta_l, \quad \text{and} \quad A_1 \leq A_2 + q_{\max}. \quad (65)$$

(b) Suppose that $f(q_c)$ is a maximum. Then (θ_l, θ_r) is invariant if and only if

$$f(q_c) < \theta_r, \text{ and } w \leq \frac{\theta_r - \theta_l}{\theta_r}. \quad (66)$$

Proof. (a) Conditions (65) amount to, respectively, $f(\theta_l) \leq \theta_r$, $\min_{\theta_l < q < \theta_r} f(q) > \theta_l$, and $f(\theta_r-) \leq \theta_r$. This way, the global minimum $f(q_c)$ lies above θ_l and the $\sup_{\theta_l < q < \theta_r} f(q)$, which is achieved at the boundary $\{\theta_l, \theta_r\}$, does not exceed θ_r .

(b) Likewise, conditions (66) amount to, respectively, $\max_{\theta_l < q < \theta_r} f(q) < \theta_r$ and $f(\theta_r-) \geq f(\theta_r) \geq \theta_l$. This time there is no condition at the left boundary (where f is always continuous) because $f(\theta_l) > \theta_l$ (see (24)). ■

From Singer's Theorem [23] one can deduce the following result [24, Proposition 1], whose formulation is adapted to our needs. Remember the definition (64) of the Schwarzian derivative $Sf(q)$.

Theorem 19 Suppose that $A_1 \leq A_2$, $[\theta_l, \theta_r]$ is invariant, and $f|_{[\theta_l, \theta_r]}$ is unimodal with $Sf|_{[\theta_l, \theta_r]}(q) < 0$ for all $q \neq q_c$. If $|f'(q^*)| \leq 1$, then $\mathcal{B}(q^*, f|_{[\theta_l, \theta_r]}) = [\theta_l, \theta_r]$.

The assumption $A_1 \leq A_2$ is needed so as $f|_{[\theta_l, \theta_r]}$ is of class C^3 (actually $f|_{[\theta_l, \theta_r]}$ is then smooth). Necessary and sufficient conditions (65) or (66) in Proposition 18 for the invariance of (θ_l, θ_r) apply also to $[\theta_l, \theta_r]$ with the changes $f(q_c) \geq \theta_l$ in (65) and $f(q_c) \leq \theta_r$ in (66). Theorem 19 holds for monotonic mappings too, though Theorem 16(a) has much weaker assumptions. Note that q^* may be a neutral fixed point in Theorem 19. Unfortunately, the implementation of the condition $Sf|_{[\theta_l, \theta_r]}(q) < 0$ in the RED dynamic is quite involved and restrictive in parametric space. This is the reason why we look out for alternative conditions.

Theorem 20 Suppose that (i) $w \leq \frac{\theta_r - \theta_l}{B - \theta_l}$, (ii) $f|_{(\theta_l, \theta_r)}$ has a local minimum at $q_c \leq q^*$ (so $f'(q^*) \geq 0$), and (iii) $A_1 \leq A_2 + q_{\max}$. Then (θ_l, θ_r) is invariant and $\mathcal{B}(q^*, f|_{(\theta_l, \theta_r)}) = (\theta_l, \theta_r)$.

Proof. By condition (i), f has a fixed point. From assumption (ii) it follows that $f|_{(\theta_l, \theta_r)}$ has at q_c a minimum with value $f(q_c) \geq q_c > \theta_l$ (otherwise, the graph of $f|_{(\theta_l, \theta_r)}$ would cross the bisector left of q_c). Apply now Proposition 18(a) to conclude the invariance of (θ_l, θ_r) .

As for the basin of attraction of q^* in (θ_l, θ_r) , consider two cases.

(a) $q_c = q^*$. Then f is increasing on $[q^*, \theta_r)$, hence it satisfies the negative feedback property (63) for every orbit $(q_n)_{n \geq 0}$ of f starting at $q_0 > q^*$. We conclude, as in the proof of Theorem 16(a), that $\lim_{n \rightarrow \infty} q_n = q^*$ for every $q_0 \in (q^*, \theta_r)$. On $(\theta_l, q^*]$ the mapping f is decreasing, so $q_0 < q^*$ implies $q_1 = f(q_0) > q^*$. Thus, $(q_n)_{n \geq 1}$ converges to q^* from the right side as well.

(b) $q_c < q^*$. Then f is increasing on $[q_c, \theta_r)$ and decreasing on $(\theta_l, q_c]$. If $q_0 \in [q_c, \theta_r)$ we are in the same situation as in the proof of Theorem 16(a) and, by the same token, $(q_n)_{n \geq 0}$ converges to q^* from the same side where q_0 lies. If, on the contrary, $q_0 \in (\theta_l, q_c)$, then $q_0 < q_c$ implies $q_1 = f(q_0) > f(q_c) > q_c$, so $(q_n)_{n \geq 1}$ converges to q^* from same side where q_1 lies (unless $q_1 = q^*$). ■

Invariance of (θ_l, θ_r) is harder to assure when $q_c > q^*$.

Theorem 21 (a) Suppose that (i) $(A_1 - A_2)^+ < q^*$, (ii) $f|_{(\theta_l, \theta_r)}$ has a minimum at $q_c > q^*$ (so $f'(q^*) < 0$), and (iii)

$$w \leq \min \left\{ \frac{\theta_r - \theta_l}{B - \theta_l}, \frac{q^* - \theta_l}{q^* - (A_1 - A_2)^+} \right\}. \quad (67)$$

If $f'(q) > -1$ for $\theta_l < q < q_c$, then (θ_l, θ_r) is invariant and $\mathcal{B}(q^*, f|_{(\theta_l, \theta_r)}) = (\theta_l, \theta_r)$.

(b) Part (a) holds also if (i) is replaced by $q^* \leq (A_1 - A_2)^+ < q_{\max}$ and (iii) is replaced by the weaker restriction

$$w \leq \frac{\theta_r - \theta_l}{B - \theta_l}. \quad (68)$$

Proof. (a) As in the proof of Theorem 20, we show first that $f(q_c) > \theta_l$. The idea is simple: since

$$f|_{(\theta_l, \theta_r)}(q) \geq (1 - w)q + w(A_1 - A_2)^+, \quad (69)$$

by (36) and q^* does not depend on the control parameter w by Theorem 6, adjust w so that $(1-w)q^* + w(A_1 - A_2)^+ \geq \theta_l$, i.e., $w \leq \frac{q^* - \theta_l}{q^* - (A_1 - A_2)^+}$. It follows that $f(q_c) \geq \theta_l$ because $q_c > q^*$. Apply again Proposition 18(a) to conclude the invariance of (θ_l, θ_r) since $w \leq \frac{\theta_r - \theta_l}{B - \theta_l}$ by (67), and $A_1 < A_2 + q^* < A_2 + q_{\max}$ by (i).

Furthermore, f is decreasing on $(\theta_l, q_c]$ and increasing on $[q_c, \theta_r]$. Therefore, the second iterate $f^2|_{(\theta_l, \theta_r)}$ is increasing. As in the proof of Theorem 16(ii), $f^2|_{(\theta_l, \theta_r)}$ has a single fixed point (at q^*) on (θ_l, q_c) (by the condition $f'|_{(\theta_l, q_c)}(q) > -1$), and no fixed point on (q_c, θ_l) (because the increasing monotonicity of f there implies $f^2(q) < q$ for $q_c \leq q \leq \theta_r$). Our claim follows similarly as in the proof of Theorem 16(b).

(b) Unlike (a), if $q^* \leq (A_1 - A_2)^+ < q_{\max}$, then $(1-w)q^* + w(A_1 - A_2)^+ \geq q^* > \theta_l$ for all $0 < w < 1$, so that no restriction on w is needed to derive $f(q_c) \geq \theta_l$. The restrictions $w \leq \frac{\theta_r - \theta_l}{B - \theta_l}$ and $A_1 < A_2 + q_{\max}$ are still needed for the invariance of (θ_l, θ_r) . The rest of the proof is the same as in (a). ■

Remark 22 *Similar results can be obtained when $f|_{(\theta_l, \theta_r)}$ has a local maximum. However, the assumptions in this case are more restrictive due to (33). Therefore, we discard this option hereafter.*

8 Implementation of the model

In the foregoing sections we have derived our main goal, $\mathcal{B}(q^*, f) = [0, B]$, under a number of different assumptions. For the implementation of these results, it is advisable to select those assumptions that are computationally expedite. We recap first the properties needed for the global stability of q^* :

- (P1) Invariance of (θ_l, θ_r) .
- (P2) $f|_{(\theta_l, \theta_r)}$ has at most one turning point.
- (P3) $\{\theta_l, \theta_r\}$ is not a periodic orbit.

Theorems 16, 20 and 21 prove then (along with Theorem 13) the global stability of q^* under different provisos; see also Theorem 19 for another approach. Moreover, we pointed out in Remark 22 the convenience of $f|_{(\theta_l, \theta_r)}$ being \cup -convex. This is also the best choice in applications because then the hypotheses of Theorems 16(b) and 21 can be somewhat simplified, as we discuss next. The first result is a straightforward upshot of the strictly increasing monotonicity of $f'|_{(\theta_l, \theta_r)}$.

Theorem 23 *If $f|_{(\theta_l, \theta_r)}$ is \cup -convex, then the hypothesis $f'|_{(\theta_l, \theta_r)}(q) > -1$ in Theorem 16(b) may be replaced by*

$$f'_+(\theta_l) = 1 - w \left(1 + \frac{\nu A_1}{2} I_{\alpha, \beta}(z(\theta_l))^{-3/2} I'_{\alpha, \beta}(z(\theta_l)) \right) \geq -1. \quad (70)$$

As for Theorem 21, set for the time being

$$f'(q^*) = 1 - mw, \quad m = 1 + \frac{\nu A_1}{2} I_{\alpha, \beta}(z(q^*))^{-3/2} I'_{\alpha, \beta}(z(q^*)) > 1, \quad (71)$$

where m does not depend on w (see (30)).

Theorem 24 *If $f|_{(\theta_l, \theta_r)}$ is \cup -convex, along with $(A_1 - A_2)^+ < q^*$ and $q_c > q^*$ (so $f'(q^*) < 0$), then the hypotheses $f'|_{(\theta_l, q_c)}(q) > -1$ and (67) in Theorem 21(a) may be replaced by (70) and*

$$w \leq \min \left\{ \frac{\theta_r - \theta_l}{B - \theta_l}, \frac{q^* - \theta_l + \frac{1}{m}(\theta_l - (A_1 - A_2)^+)^+}{q^* - (A_1 - A_2)^+} \right\}, \quad (72)$$

respectively.

Proof. The purpose of the restriction $w \leq \frac{q^* - \theta_l}{q^* - (A_1 - A_2)^+}$ in Equation (67) is to assure that $f(q_c) > \theta_l$. Convexity can be exploited to weaken this bound (see the second term in (72)). The proof is geometrical on the Cartesian plane $\{(q, y) \in \mathbb{R}^2\}$.

Since $f|_{(\theta_l, \theta_r)}$ is \cup -convex, the curve $y = f(q)$, $q^* \leq q < \theta_r$, lies on the upper-right side of the tangent to $y = f(q)$ at the point $q = q^*$, whose equation is $y = -sq + (s+1)q^*$ with $0 < s = s(w) := |f'(q^*)| < 1$. This tangent cuts the baseline $y = \theta_l$ of the square $[\theta_l, \theta_r] \times [\theta_l, \theta_r]$ at the point $q_{\text{cut,tan}}(w) = \frac{q^*(s+1) - \theta_l}{s} = q^* + \frac{q^* - \theta_l}{s} > q^*$. By (71),

$$q_{\text{cut,tan}}(w) = \frac{q^*mw - \theta_l}{mw - 1}$$

since $s = -f'(q^*) = mw - 1 > 0$.

On the other hand, the lower envelope $y = (1-w)q + w(A_1 - A_2)^+$ (Proposition 2) cuts the baseline $y = \theta_l$ at

$$q_{\text{cut,env}}(w) = \frac{\theta_l - w(A_1 - A_2)^+}{1-w}.$$

If $q_{\text{cut,env}}(w) \leq q_{\text{cut,tan}}(w)$, we are done because then $f(q_c) > \theta_l$, so (θ_l, θ_r) is invariant by (65). Furthermore, we require $q_{\text{cut,env}}(w) \geq q^*$ to improve (67). The second bound in (72) amounts precisely to both conditions. ■

Remark 25 *If $m \rightarrow \infty$ in (72), then we recover (67), as it should.*

Proposition 4 gives the sufficient condition

$$3J_{\alpha,\beta}(z(q)) - 2h_{\alpha,\beta}(z(q)) > 0, \quad (73)$$

for $f|_{(\theta_l, \theta_r)}$ to be \cup -convex, where $J_{\alpha,\beta}(z(q)) = I_{\alpha,\beta}(z(q))^{-1}I'_{\alpha,\beta}(z(q)) > 0$ for $z(\theta_l) < z < z(\theta_r)$ (see (73)), and

$$h_{\alpha,\beta}(z) = \frac{\alpha - 1}{z} - \frac{\beta - 1}{1 - z} = \frac{\alpha - 1 - (\alpha + \beta - 2)z}{z(1 - z)} \quad (74)$$

(see (38)). We are going to translate condition (73) into convexity regions for $f|_{(\theta_l, \theta_r)}$ in the (α, β) -plane.

Proposition 26 *$f|_{(\theta_l, \theta_r)}$ is \cup -convex in the following cases, where $z(q) = \nu(q - q_{\min}) \in (0, 1)$:*

- (a) $\beta < 1$, $\alpha < 1$, $0 < z(q) \leq \frac{\alpha - 1}{\alpha + \beta - 2}$.
- (b) $\beta \geq 1$, $\alpha \leq 1$, $0 < z(q) < 1$.
- (c) $\beta > 1$, $\alpha > 1$, $\frac{\alpha - 1}{\alpha + \beta - 2} \leq z(q) < 1$.

Proof. Solve the inequality $h_{\alpha,\beta}(z) \leq 0$ with $0 < z < 1$, and apply (73) to conclude $f''|_{(\theta_l, \theta_r)}(q) > 0$. ■

Comparison with Example 8 (which shows that $f|_{(\theta_l, \theta_r)}$ is \cup -convex for $\beta = 1$ and $\alpha > 0$) suggests that the sufficient conditions in Proposition 26 are, beside incomplete, rather conservative. The following lemma provides a more useful result.

Proposition 27 *$f|_{(\theta_l, \theta_r)}$ is \cup -convex in the following cases, where $z(q) = \nu(q - q_{\min}) \in (0, 1)$:*

- (a) $\alpha \leq \beta$ and $0 < z(q) < \frac{\alpha}{\alpha + \beta}$.
- (b) $\alpha > \beta$ and $0 < z(q) < \frac{\alpha + 2}{\alpha + \beta + 4}$.

Proof. According to Inequality (27) in [25], we obtain that, for $z < \frac{\alpha}{\alpha + \beta}$,

$$I_{\alpha,\beta}(z) < \frac{z^\alpha(1-z)^\beta}{\mathfrak{B}(1; \alpha, \beta)(\alpha - (\alpha + \beta)z)} = I'_{\alpha,\beta}(z) \frac{z(1-z)}{\alpha - (\alpha + \beta)z},$$

which implies

$$2h_{\alpha,\beta}(z(q)) - 3I_{\alpha,\beta}(z)^{-1}I'_{\alpha,\beta}(z) < 2h_{\alpha,\beta}(z(q)) - 3 \frac{\alpha - (\alpha + \beta)z}{z(1-z)}.$$

Use (74) to conclude that the condition (73) is satisfied when

$$\frac{(\alpha + \beta + 4)z - \alpha - 2}{z(1-z)} < 0$$

where $z < \frac{\alpha}{\alpha + \beta}$. ■

Corollary 28 $f|_{(\theta_l, \theta_r)}$ is \cup -convex whenever

$$z(\theta_r) = \frac{\theta_r - q_{\min}}{q_{\max} - q_{\min}} \leq \begin{cases} \frac{\alpha}{\alpha + \beta} & \text{if } \alpha \leq \beta, \\ \frac{\alpha + 2}{\alpha + \beta + 4} & \text{if } \alpha > \beta. \end{cases}$$

Example 29 To check numerically Proposition 27 and Corollary 28, consider the RED model with $\alpha = 1$, $\beta \ll 1$ (this case is not covered by Proposition 26) and approximate

$$I_{1,\beta}(x) = 1 - (1-x)^\beta = -\beta \ln(1-x) + O(\beta^2)$$

on $[0, 1 - \varepsilon]$, $\varepsilon \ll 1$, by

$$I_{1,\beta}(x) = -\beta \ln(1-x) = \beta \ln \frac{1}{1-x},$$

hence

$$I'_{1,\beta}(x) = \frac{\beta}{1-x}, \quad I_{1,\beta}^{-1}(y) = 1 - e^{-y/\beta}.$$

In this case $f|_{(\theta_l, \theta_r)}$ is \cup -convex, i.e.,

$$3J_{\alpha,\beta}(z) - 2h_{\alpha,\beta}(z) = -\frac{\beta}{(1-z)^2} \left(\frac{3}{\ln(1-z)} + 2 \right) > 0,$$

if and only if

$$z < 1 - e^{-3/2} \simeq 0.7769$$

for all $\beta \ll 1$. According to Proposition 27(b), $f|_{(\theta_l, \theta_r)}$ is \cup -convex if

$$z < \frac{3}{\beta + 5} \lesssim 0.6.$$

This is an acceptable result regarding the application sought.

9 Numerical simulations

Our numerical simulations comprise a simple benchmarking against the original RED model (Section 9.1) and a scan of the (α, β) -plane to quantify the robustness of both the stationary drop probability and the bifurcation point of the averaging weight (Section 9.2). The simulation scenario is discussed in Section 9.3. Owing to the many parameters of the RED model, we have to content ourselves with illustrating the results with a few representative picks. The computer codes were written with Python.

9.1 Benchmarking RED vs generalized RED

To compare the generalized RED model with the original one [5] we have chosen the bifurcation points of $A_1 = NK/\sqrt{p_{\max}}$, $A_2 = Cd/M$ and w . As explained in Section 5, the bifurcation points of other parameters can be then obtained from $A_{1,\text{bif}}$ or $A_{2,\text{bif}}$ by fixing the rest of them. In particular, the number of users N (included in A_1) and the round trip time d (included in A_2) are relevant system parameters with regard to congestion control because they change actually in real time. Remember that q^* does not depend on w and it exists as long as $A_1 < A_2 + q_{\max}$ (Theorem 6).

Figures 3, 4 and 5 show bifurcation diagrams with respect to A_1 , A_2 and w obtained with $\alpha = 0.5$, $\beta = 0.2$ (left panels) and $\alpha = \beta = 1$ (right panels). The settings of the other control parameters are given in the captions of the figures. The parametric grid used for the bifurcation diagrams has 2000 points; the orbits were 550 iterates long, the first 500 (the transient) having been discarded. In all panels, the initial 2-cycle after the bifurcation point (in the positive/negative direction for the direct/reverse bifurcations) ends when the cycle collides with the right threshold θ_r . From then on, the dynamical core (θ_l, θ_r) is no longer invariant, as shown by the fact that the orbits visit also points beyond θ_r , seemingly filling up a longer and longer interval that eventually hits the left threshold θ_l .

In Figure 3, the system parameters not affecting A_1 are fixed as follows:

$$C = 321,000 \text{ kBps}, \quad d = 0.012 \text{ s}, \quad M = 1 \text{ kB}, \quad B = 2000 \text{ packets}. \quad (75)$$

Comparison of both panels shows that $A_{1,\text{bif}}$ is smaller in the generalized model ($\simeq 1450$ vs $\simeq 1950$). From a practical point of view, it is more useful if the bifurcation point $A_{1,\text{bif}}$ is as small as possible, so that $N_{\text{bif}} = \sqrt{p_{\max}} A_{1,\text{bif}}/K$ is also as small as possible. This is a desired situation since a smaller number of connections (users) tends to disrupt the

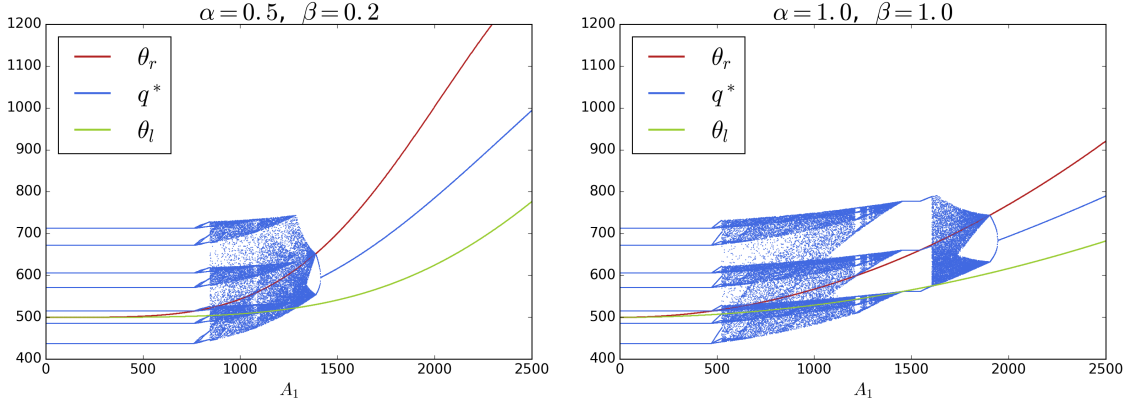


Figure 3: Bifurcation diagram of the average queue length with respect to the parameter A_1 for the values of α and β shown on the top of the panels. System parameters are given in (75). Other control parameters: $q_{\min} = 500$, $q_{\max} = 1500$ and $w = 0.15$. The constant A_2 is 3852 and A_1 ranges in the interval $[0, 2500]$.

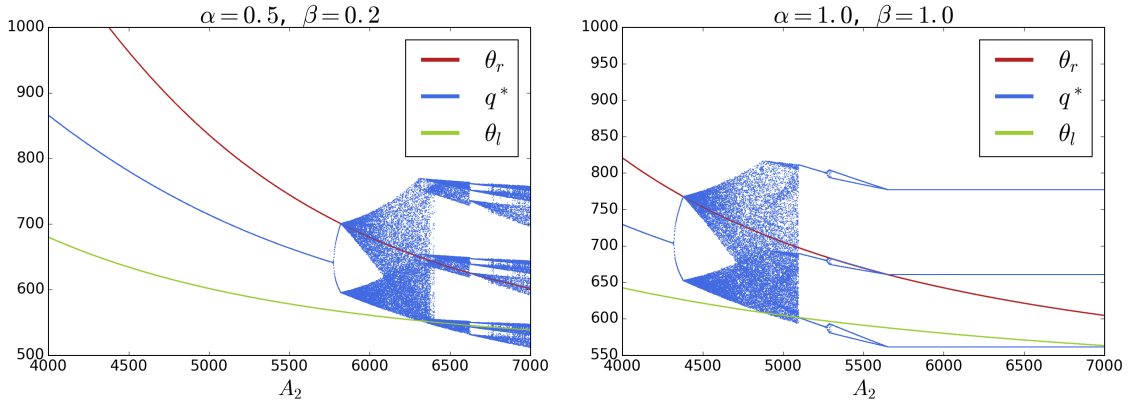


Figure 4: Bifurcation diagram of the average queue length with respect to the parameter A_2 for the values of α and β shown on the top of the panels. System parameters are given in (76). Other control parameters: $q_{\min} = 500$, $q_{\max} = 1500$, $w = 0.15$ and $p_{\max} = 1$. The constant A_1 is 2265.8 and A_2 ranges in the interval $[4000, 7000]$.

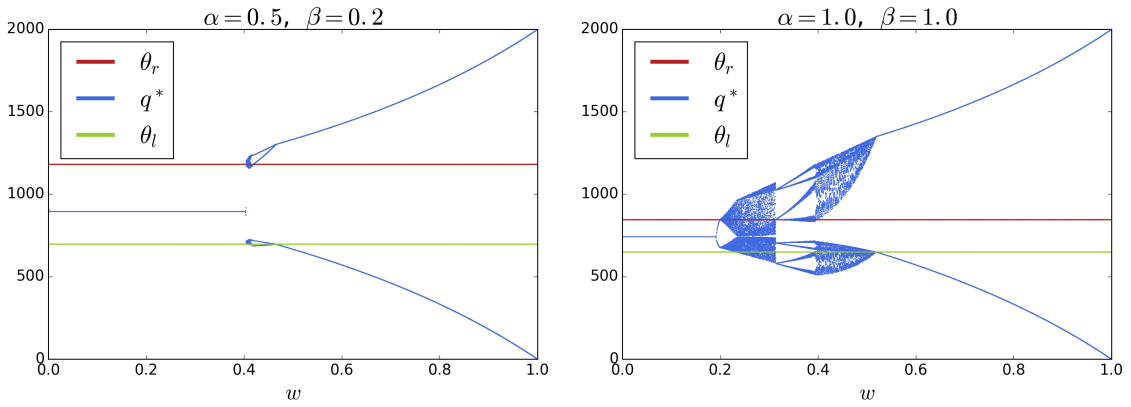


Figure 5: Bifurcation diagram of the average queue length with respect to the parameter w for the values of α and β shown on the top of the panels. System parameters are given in (28). Other control parameters: $q_{\min} = 500$, $q_{\max} = 1500$ and $p_{\max} = 1$. The parameter w ranges in the interval $[0, 1]$. The constant A_1 is 2265.8 and A_2 is 3852.

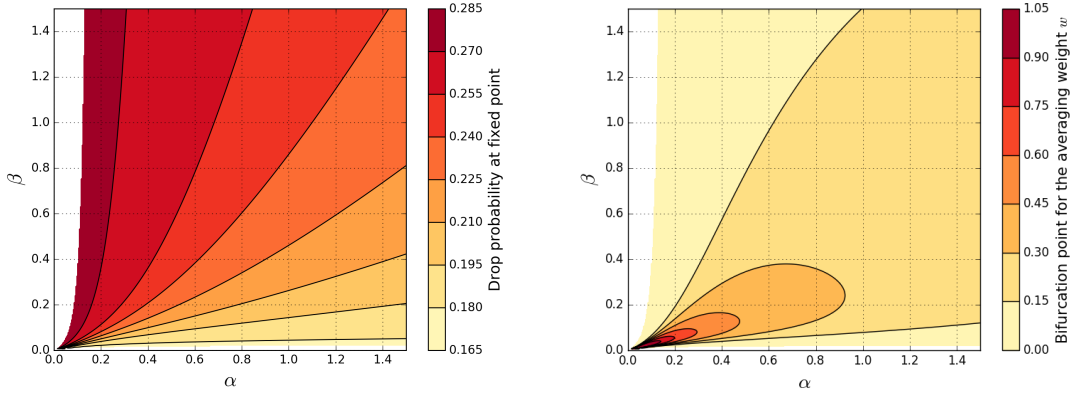


Figure 6: (α, β) -parametric sweeps reveal the robustness domains for both the drop probability at the fixed point (left) and the bifurcation point for the averaging weight (right).

dynamic [5]. When the dynamical core (θ_l, θ_r) is so small that the asymptotic orbits do not visit it any more, we see a stable 7-cycle emerge at the left end of both panels. This orbit is obviously independent of A_1 .

In Figure 4, the system parameters not included in A_2 are fixed as follows:

$$N = 1850, \quad K = 1.2247, \quad B = 2000 \text{ packets.} \quad (76)$$

Comparison of both panels shows that $A_{2,\text{bif}}$ is greater in the generalized model ($\simeq 5750$ vs $\simeq 4350$). Contrarily to the previous case, this time it is advisable that the bifurcation point is as large as possible since large time delays $d = A_2 M / C$ favors the instability of the system [5]. In the right half of the right panel we see a 3-cycle that is independent of A_2 . This orbit circles around (θ_l, θ_r) without visiting it.

For Figure 5, all system parameters are fixed as in (28). Comparison of both panels shows that w_{bif} is greater in the generalized model ($\simeq 0.4$ vs $\simeq 0.2$). In this case, the greater the bifurcation point the more stable the system will be. As w approaches 1, the orbits jump between an ever fuller buffer and an ever emptier buffer, since incoming packets are alternatively accepted or dropped with an ever higher probability (see (1) and (2))

The results shown in Figures 3–5 are also representative of other bifurcation diagrams calculated by the authors. In any case, we may conclude that an adequate setting of the control parameters α and β can extend the stability interval of the RED dynamics beyond the bifurcation points $A_{1,\text{bif}}$, $A_{2,\text{bif}}$ and w_{bif} in the original RED model.

9.2 Robustness domains in the (α, β) -plane

Finding particular values of α and β that improve the stability of the RED dynamics in the light of, for instance, bifurcation diagrams (as we did in Section 9.1) is not sufficient to design an AQM mechanism. Those values of α and β must be also robust, meaning that small changes do not appreciably degrade the stability of the system. This caveat is not only necessary to cope with the physical and numerical noise of the intended algorithmic implementation, but also to make the control feasible under changing system parameters.

To quantify the robustness of RED model we have scanned the interval $[0.002, 1.5] \times [0.002, 1.5]$ of the (α, β) -plane with precision $\Delta\alpha = \Delta\beta = 3.745 \times 10^{-3}$ (corresponding to a grid of 400×400 points), and for each point (α, β) we have calculated (i) the stationary drop probability ($p^* = I_{\alpha,\beta}(z(q^*)) \cdot p_{\text{max}}$, Equation (13)) and (ii) the bifurcation point of the averaging weight w_{bif} (Equations (49)-(50)).

The left panel of Figure 6 shows a color map of p^* where same-color-regions correspond to stationary drop probabilities within bins of size 0.015 (see the color scale along the right side). The right panel of Figure 6 displays the same information for w_{bif} with bins of size 0.15; points with $w_{\text{bif}} \geq 1$ correspond to systems without bifurcations with respect to w . In both cases, the system parameters are tuned as in (28). Note that Figure 5 corresponds to the points $(\alpha, \beta) = (0.5, 0.2)$ (left panel) and $(\alpha, \beta) = (1, 1)$ (right panel) of the right panel of Figure 6. Therefore, both configurations are robust.

The above and similar figures make it clear that not all choices for α and β are equally good when real stability enters the scene. First of all, points (α, β) close to the boundaries of the robustness (same-color) domains should be avoided. Also, the larger the robustness domain, the better from the viewpoint of stability. In the end, the choice of

α, β and other control parameters will be a trade-off between the extent of the corresponding robustness domain and the operational parametric ranges. Thus, although the greatest robustness domain for w_{bif} (Figure 6, right panel)) corresponds to $0.15 \leq w_{\text{bif}} \leq 0.30$, the possibly best choice for α, β belongs to the core of the domain pertaining to the bin $0.25 \leq w_{\text{bif}} \leq 0.50$, because it leaves an acceptable range $0 < w < 0.25$ for a stable operation of the congestion control algorithm.

9.3 Discussion

In Sections 9.1 and 9.2 we used a simulation scenario (Figure 1) parametrized with data obtained from the Miguel Hernández University network, where an outbound bottleneck link is shared by many connections to different Spanish websites. In this scenario, we interpreted the shared link as an outbound Internet link with capacity C and assumed a set of N connections having uniformly an average round-trip propagation delay d (without any queueing delay). Rather than interpreting this assumption as a requirement that the connections must have the same propagation delay, we consider d as the effective delay that represents the overall propagation delay of the connections or, alternatively, this could describe a case where the outbound bottleneck link has a propagation delay that dominates the round-trip delays of the connections as studied in [5]. Then, the literature acknowledges that identification and classification of network traffic is an important prerequisite of network management [26]. In this scenario, the packet length was analyzed through a statistical distribution of packet length M among applications using web traffic over TCP protocol.

Concerning the numerical results, the robustness maps introduced in Section 9.2 encapsulate the perhaps most important information needed to set up an actual AQM algorithm based on the analysis and results of this paper. Indeed, they not only tell us, for example, what the bifurcation points of different parameters are as a function of α and β but, equally important, how robust those parameters are with respect to changes in α, β possibly due to internal noise and external sources. A related decision to make is which the relevant parameters are, i.e., what parameters to monitor and what control parameters to act on; certainly, N and w belong to them. The ideally best choices lie in the core of the largest robustness domains, but other practical issues such as the variation ranges left for relevant control parameters might advise otherwise. This situation was illustrated in Section 9.2 with w_{bif} .

10 Conclusion and outlook

The main role of an AQM is to control the queue size at a router buffer under stable conditions to avoid data flow congestion. In the quest for ever better AQM algorithms, we have presented in Section 3 and studied in Sections 4–9 a discrete-time dynamical formulation of RED. Our model generalizes a model proposed by Ranjan et al. [5] in that we replace the probability distribution (4) by the beta distribution $I_{\alpha, \beta}$ (13); for $\alpha = \beta = 1$ we recover the original model. The expectation in so doing is a better performance of the ensuing AQM mechanism in terms of global stability and parametric robustness thanks to the additional control parameters α and β . We went also beyond the analysis in [5] in some formal, though important, respects including: restriction on system parameters for the existence of the dynamical core (θ_l, θ_r) ($A_1 < A_2 + B$, Proposition 1); parameter restriction for the existence of a fixed point ($A_1 < A_2 + q_{\text{max}}$, Theorem 6); consideration of a discontinuous dynamic ($A_1 > A_2$) throughout the paper; and parameter restrictions for (θ_l, θ_r) to be invariant both in the monotonic case (Proposition 14) and unimodal case (Theorems 20 and 21).

The main theoretical results obtained in this paper, which are summarized at the beginning of Section 8, concern the global stability of the generalized RED dynamics (17). For this reason, the most important results referred to the stability properties of the unique fixed point q^* (Section 5) and the settings of the control parameters α, β and w that guarantee its global attractiveness (Section 7). Based on these results, we have derived also a number of practical guidelines regarding stability domains in the (α, β) -plane (Section 8) and, most importantly, robust settings for those parameters (Section 9.2). The generality and formulation of the theoretical results was commensurate with their applicability to an AQM algorithm. In this sense we can speak of a feedback from the practical to the theoretical sections. Benchmarking against the original dynamical model in Section 9.1 confirms that the control leverage introduced by the parameters α and β improves the stability of the RED dynamics. Further practical aspects were discussed in Section 9.3.

To conclude, the general purpose of this paper was to pave the way for the implementation of the RED model (17) as an AQM algorithm. To this end, we have addressed in the preceding sections the basic theoretical and practical aspects of the RED dynamics related to global stability. The implementation of these results under real conditions is the subject of current research.

Acknowledgements

We thank our referees for their constructive criticism. We are also grateful to José Ramón García Valdés, network administrator of the Miguel Hernández University communication network, for the data (28). This work was financially

supported by the Spanish Ministry of Science, Innovation and Universities, grant MTM2016-74921-P (AEI/FEDER, EU).

References

- [1] R. Adams, Active queue management: A survey, *IEEE Communications Surveys and Tutorials* 15, 1425-1476, 2013.
- [2] S. Floyd and V. Jacobson, Random early detection gateways for congestion avoidance, *IEEE/ACM Trans. Networking* 1, 397-413 (1993).
- [3] S. Athuraliya, S. Low, V. H. Li, and Q. Yin, REM: active queue management, *IEEE Network* 15, 48–53, 2001.
- [4] R. J. La and V. Anantharam, Utility-based rate control in the Internet for elastic traffic, *IEEE/ACM Trans. Networking* 10, 272–286, 2002.
- [5] P. Ranjan, E.H. Abed and R.J. La, Nonlinear Instabilities in TCP-RED, *IEEE/ACM Transactions on Networking* 12, 1079-1092, 2004.
- [6] W. de Melo and S. van Strien, *One-Dimensional Dynamics*, Springer Verlag, Berlin, 1993.
- [7] H. Thunberg, Periodicity versus chaos in one-dimensional dynamics, *SIAM Rev.* 43, 3-30, 2001.
- [8] G. Duran, J. Valero, J.M. Amigó, A. Giménez, and O. Martínez-Bonastre, Stabilizing chaotic behavior of RED. 2018 IEEE 26th International Conference on Network Protocols, 241-242, Sept. 2018.
- [9] G. Duran, J. Valero, J.M. Amigó, A. Giménez, and O. Martínez-Bonastre, Bifurcation analysis for the internet congestion, 2019 IEEE Infocom.
- [10] S. Patel, Performance analysis of RED for stabilized queue. In: 2014 seventh international conference on contemporary computing (IC3); 2014. p. 306–11.
- [11] C.W. Feng, L.F. Huang, C. Xu, Y.C. Chang, Congestion control scheme performance analysis based on nonlinear RED. *IEEE Syst J* 2017;11(4):2247–54.
- [12] Karmeshu, S. Patel, S. Bhatnagar, Adaptive mean queue size and its rate of change: queue management with random dropping. *Telecommun Syst* 2017;65(2):281–95.
- [13] S. Patel, Karmeshu, A new modified dropping function for congested AQM networks. *Wirel Pers Commun* 2019;104(1):37–55.
- [14] W. Wang, H. Wang, W. Tang and F. Guo, A new approach to estimate RED parameters using function regression, *International Journal of Future Generation Communication and Networking* 7, 103-118, 2014.
- [15] M. Mathis, J. Semke, J. Mahdavi, and T. Ott, The macroscopic behavior of the TCO congestion avoidance algorithm, *Computer Communication Review* 27 (3), 1997.
- [16] L.J. Pei, X.W. Mu, R.M. Wang, and J.P. Yang, Dynamics of the Internet TCP-RED congestion control system, *Nonlinear Analysis: Real World Applications* 12, 947-955 (2011).
- [17] M. Abramowitz and I. Stegun, *Handbook of Mathematical Functions*, Dover Publications, New York, 1972.
- [18] A.N. Sharkovsky, Coexistence of cycles of a continuous map of the line into itself, *Ukrainian Mathematical Journal* 16, 61-71, 1964.
- [19] T. Li and J.A. Yorke, Period three implies chaos, *Amer. Math. Monthly* 82, 985-992, 1975.
- [20] M. Misiurewicz and W. Szlenk, Entropy of piecewise monotone mappings, *Studia Math.* 67, 45-63, 1980.
- [21] J.M. Amigó and A. Giménez, A simplified algorithm for the topological entropy of multimodal maps, *Entropy* 16, 627-644, 2014.
- [22] J.M. Amigó and A. Giménez, Formulas for the topological entropy of multimodal maps based on min-max symbols, *Discrete and Continuous Dynamical Systems B* 20, 3415-3434, 2015.
- [23] D. Singer, Stable orbits and bifurcations of maps of the interval, *SIAM J. Appl. Math.* 35, 260-267, 1978.
- [24] H.A. El-Morshedy and E. Liz, Globally attracting fixed points in higher order discrete population models, *J. Math. Biol.* 53, 365-384, 2006.
- [25] J. Segura, Sharp bounds for cumulative distribution functions, *J. Math. Anal. Appl.* 436, 748-763, 2016.
- [26] Xiao-Long Wu, Wei-Min Li, Fang Liu, and Hua Yu. Packet size distribution of typical Internet applications. In 2012 International Conference on Wavelet Active Media Technology and Information Processing (ICWAMTIP), pages 276–281, December 2012.